[2]Falkner, V. M., "A Further Investigation of the Boundary-Layer Equations," British Aero. Res. Council, Reports and Memoranda, Rept. 1884, 1937.
[3]Smith, A. M. O., "Improved Solutions of the Falkner and Skan Boundary Layer Equations," Rep. E. S. 16009 [Contract a(s) 9027], Douglas Aircraft Co. Inc., 1952.
[4]Evans, H. L., *Laminar Boundary Layer Theory*, Addison–Wesley, London, 1968.
[5]Radbill, J. R., "Application of Quasilinearization to Boundary-Layer Equations," *AIAA Journal*, Vol. 2, 1964, pp. 1860–1862.
[6]Libby, P. A., and Chen, K. K., "Remarks on Quasilinearization Applied in Boundary Layer Calculations," *AIAA Journal*, Vol. 4, 1966, pp. 937–939.
[7]Libby, P. A., and Liu, T. M., "Further Solutions of the Falkner-Skan Equation," *AIAA Journal*, Vol. 5, 1967, pp. 1040–1042.
[8]Stewartson, K., *The Theory of Laminar Boundary Layers in Compressible Fluids*, Oxford Mathematical Monographs, Oxford Univ. Press, Oxford, 1964.
[9]White, F. M., *Viscous Fluid Flow*, McGraw–Hill, New York, 1991.
[10]Coppell, W., *Philosophical Transactions of the Royal Society of London, Series A: Mathematical and Physical Sciences*, Vol. 253, 1960, p. 101.

M. Sichel
Associate Editor

Evolution Strategies for Automatic Optimization of Jet Mixing

Petros Koumoutsakos*
Swiss Federal Institute of Technology, CH-8092 Zurich, Switzerland
Jonathan Freund†
University of California, Los Angeles, Los Angeles, California 90095-1597
and
David Parekh‡
Georgia Tech Research Institute, Atlanta, Georgia 30080

I. Introduction

EVOLUTION strategies (ES) are introduced for the optimization of active control parameters for enhancing jet mixing. It is shown that the evolution algorithms can identify, in an automated fashion, not only previously known effective actuations but also find good but previously unidentified parameters. In this study, simulations of model jets are used to demonstrate the feasibility of the methods. ES are robust, highly parallel, and portable algorithms that may be most useful in an experimental setting at realistic Reynolds numbers. Simulations of inviscid incompressible flows using vortex models, as well as direct numerical simulations (DNS) of very low-Reynolds-number compressible flows, are used in this study to evaluate different forcing parameters.

Our objective is twofold: 1) explore the possibility of ES to find previously identified modes of efficient operation and 2) discover previously unknown effective actuations. Practical engineering concerns will dictate the choice of actuator parameters and relevant cost functions. In Sec. II, we present a description of the ES; in Sec. III, we present results from the application of these to the optimization of compressible jets and vortex models. Section IV is a discussion of results and an outline for future research.

Received 9 August 2000; revision received 16 January 2001; accepted for publication 18 January 2001.

*Professor, Institute of Computational Sciences; petros@inf.ethz.ch.
†Assistant Professor, Department of Mechanical and Aerospace Engineering; jfreund@ucla.edu. Member AIAA.
‡Director, Aerospace, Transportation, and Advanced Systems Laboratory, Georgia Tech Research Center; david.parekh@gtri.gatech.edu. Member AIAA.

II. Evolution Strategies

ES are continuous parameter optimization techniques based on principles of evolution such as reproduction, mutation, and selection. We define a vector in the control parameter space $\boldsymbol{x} = (x_1, x_2, \ldots, x_M)$ as an individual and a set of such individuals as a population. ES use a fitness value, prescribed by $F(\boldsymbol{x}) = F(x_1, x_2, \ldots, x_M)$, to identify the best individual from a population. We take better individuals to have larger F values.

A. Two-Membered ES

The simplest ES has a population with two competing individuals, a two-membered strategy. Evolution occurs by mutation and selection, the two operations that Darwin considered the most important in the evolution of species. Each individual is represented by a pair of real vectors $\boldsymbol{u} = \boldsymbol{u}(\boldsymbol{x}, \boldsymbol{\sigma})$, where $\boldsymbol{\sigma}$ is an M-dimensional vector of standard deviations.

Following Rechenberg,[1] the optimization algorithm is as follows:

1) Initialization is where a parent genotype consisting of M genes is specified initially as $\boldsymbol{x}^0$.

2) Mutation is when the parent of generation n produces a descendant with slightly different genotype. The operation of mutation is realized by modifying $\boldsymbol{x}_p$ according to $\boldsymbol{x}_c^n = \boldsymbol{x}_p^n + \mathcal{N}(\boldsymbol{\sigma}_p^n)$, where $\mathcal{N}(\boldsymbol{\sigma})$ is an M-dimensional vector of normal random number with zero mean and standard deviations $\boldsymbol{\sigma}$.

3) Selection is where the fittest individual according to its F value becomes the parent of the next generation:

$$\boldsymbol{x}_p^{n+1} = \begin{cases} \boldsymbol{x}_p^n, & \text{if } F\left(\boldsymbol{x}_p^n\right) \geq F\left(\boldsymbol{x}_c^n\right) \\ \boldsymbol{x}_c^n, & \text{otherwise} \end{cases} \tag{1}$$

The variance of the population members is adjusted using the one-fifth success rule proposed by Rechenberg: If more than one in five offsprings result in an improved solution, then the variance is increased.[1] For regular optimization problems[2] the method is known to converge to a global minimum, but the rate of convergence cannot be anticipated. Therefore, in finite time there is, of course, no guarantee that the global optimum has been reached, a trait shared by all optimization techniques. Schwefel[3] provides a complete description of the algorithm.

B. Parameter Constraints

In problems of active flow control, engineering considerations impose constraints on the actuation parameters. Such constraints are formulated as inequalities, such as $C_j(\boldsymbol{x}) \geq 0$. In this work descendants that do not satisfy the constraints are treated as unsuccessful mutations.

III. Jet Flows Optimization

A. Optimized Excitation of Compressible Jets

DNS of the developing region of compressible jets forced by slot-jet fluidic actuators are used to evaluate the fitness of individuals. The compressible flow equations were solved directly using a combination of sixth-order compact finite differences, spectral methods, and fourth-order Runge–Kutta time advancement. Further details of the numerical algorithm and techniques for including two slot-jet actuators that each span 90 deg of the jet (on opposite sides) just downstream of the nozzle were reported elsewhere.[4] Despite the low Reynolds number dictated by the computational expense (only $Re = 500$ in this study) the actuators were able to induce the gross effects observed in experiments at much higher Reynolds numbers.[5] A path to implementation at more relevant flow conditions is discussed in Sec. IV.

For this study, only three actuation parameters were varied: amplitude, frequency, and phase. The actuation is taken as a sum of harmonic waveforms:

$$v_r = -\min\left(\sum_{i=1}^{N} A_i\left[1 + \sin\left(U_j \frac{Sr_i}{D} t + \phi_i\right)\operatorname{sgn}[\cos\theta]\right], \frac{U_j}{2}\right) \tag{2}$$

where v_r is the radial velocity at the actuator exit, U_j is the jet exit velocity, A_i are the amplitudes, Sr_i are the Strouhal numbers, and

ϕ_i are the phases of the different modes. The sgn[cos(θ)] factor causes each waveform to excite a flapping mode in the jet. Note that the phases ϕ_i are the relative phases of the different modes; the two actuators always acted 180 deg out of phase. The A_i were constrained to be nonnegative, and the Sr_i were restricted to be $0 \le Sr \le 0.8$. The relative phases were not constrained.

The computational mesh was $112 \times 42 \times 16$ in the streamwise, radial, and azimuthal direction, respectively, and the computational domain extended to $16r_0$ downstream and $5r_0$ in the radial direction, where r_0 is the jet radius. A stretched-mesh boundary zone was positioned in $x > 8r_0$ and $r > 3.5r_0$ to absorb out-flowing fluctuations.[4] In each iteration of the optimization, the jet was simulated starting from an unforced case for several periods of forcing after the passing of initial transients. Because the flow is laminar and becomes quasi periodic, this was sufficient to provide a measure of the long-time actuator effectiveness. In total, 200 iteration were made.

Three waveforms ($N = 3$) were used. The initial parameters and the parameters that maximized F are shown in Table 1. The fitness function was defined as

$$F = \int_{4r_0}^{8r_0} \int_0^{2\pi} \int_0^{3.5r_0} v_r^2 r \, \mathrm{d}r \, \mathrm{d}\theta \, \mathrm{d}x \tag{3}$$

which was evaluated using a trapezoidal rule quadrature and increased by a factor of 10 for the best parameters.

Note that the evolution strategy reduced the amplitude of two of the wave modes to a very low level giving effectively the same excitation that was shown to be successful in experiments[5] and in higher Reynolds number simulations on larger meshes.[4] This also demonstrates the mesh independence of the computation and its accuracy, at least for this measure of mixing. Notice also that the maximum amplitude stayed below half the jet velocity indicating that a sinusoidal profile was preferable to one that was clipped by the maximum amplitude constraint in Eq. (2). Scalar mixture fraction is shown in Fig. 1 for the initial and best cases. The best case clearly shows high-amplitude flapping.

Table 1 Initial and best actuation parameters

Initial			Best		
A_i/U	Sr_i	ϕ_i	A_i/U	Sr_i	ϕ_i
0.45	0.50	0.00	0.04	0.33	0.54
0.40	0.20	0.70	0.42	0.17	0.31
0.35	0.50	1.00	0.07	0.45	1.57

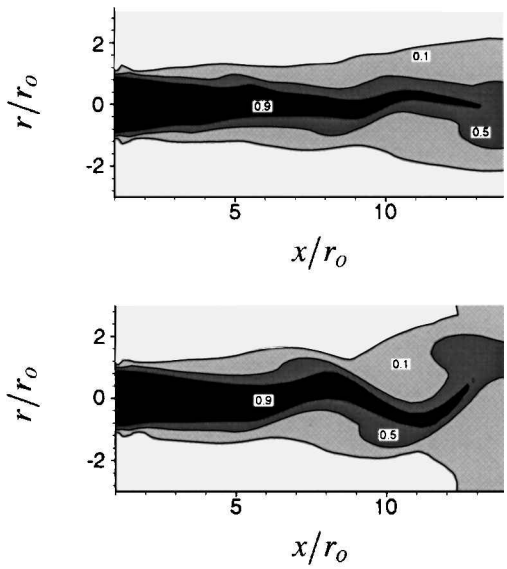

Fig. 1 Jet fluid mixture fraction with the initial (top) and best (bottom) parameters.

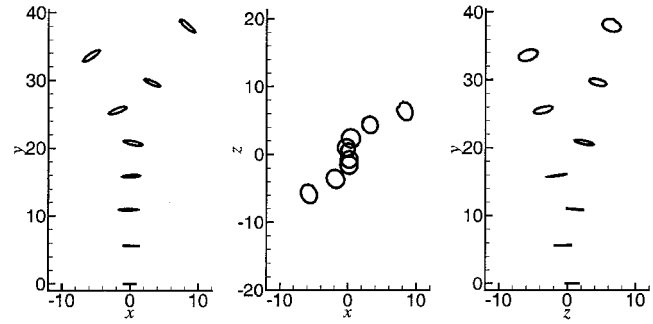

Fig. 2 Vortex filament positions in the hybrid bifurcating jet with $Sr_a = 0.28$, $A_h = 0.63$, $\beta = 2$, and $\phi = 0$.

B. Incompressible Vortex Model

In these simulations, it is assumed that the effects of compressibility and viscosity do not affect the flow dynamics and that the circular jet is modeled by the combination of discrete vortex filaments and a fixed semi-infinite cylindrical sheet of vorticity with circulation per unit length γ that represents the nozzle. Helical excitation as used in the experiments of Lee and Reynolds[6] is modeled by rotating the axis of the vortex cylinder with displacement A_h/r_0 about the nominal jet centerline. The rotation frequency is denoted by f_h, and the axial frequency is defined as $f_a = Sr_a\gamma/2r_0$. The frequency f_a is the rate at which filaments are generated at the origin. The velocities induced by each filament and the vortex sheet are added to determine the trajectory of each filament. Sr_a sets the time between creation of new rings. The circulation of each shed filament is $\gamma = Sr_a\Gamma/R$. Here β fixes the ratio of the axial to orbital excitation, and ϕ sets their relative phase. Further details of this model and its numerical implementation were reported by Parekh et al.,[7] who also provided a detailed validation of the method through direct comparison with bifurcating jet experiments and refinements of the vortex ring representations.[6]

The control parameters were constrained so that $0 \le A_h \le 1$, $0.1 \le Sr_a \le 1$, $0.2 \le \beta \le 5$, and $0 \le \phi \le 2\pi$. The fitness function was the average angle of the ring trajectories defined as the angle between the jet centerline and the line that connects the center of the jet exit to the centroid of the vortex ring nodes. This metric was evaluated after 11 periods of axial excitation.

Initially we expected the algorithm to select a jet that bifurcates in a single plane with values of Sr_a and A_h that maximize the spreading angle as seen in laboratory jets.[6] Instead, a jet flow was found that had never been observed in previous experiments or calculations. It initially resembles a bifurcating jet (Fig. 2), but several diameters downstream, the two branches of the jet exhibit a secondary bifurcation in which the rings change direction by about 45 deg. This results in a wide spreading angle, as seen in Fig. 2. Unfortunately, the parameters that lead to this double bifurcation have not been tested experimentally and so the code cannot be validated for this case as is was for the other cases.[7] Regardless, the possibility that ES can identify novel control parameters has been demonstrated.

IV. Conclusions

Given the variety of different forcing schemes, cost functions, and flows to be controlled, it is impossible to anticipate the best optimization scheme for any particular case, but the present results clearly demonstrate that ES can be a valuable tool for jet mixing optimization. They identified, in an automated fashion, previously known flow controls and found previously unknown parameters that further enhance spreading. Their strength is their portability, which is considered particularly attractive for problems such as jet noise control flow where the mechanisms appear too poorly understood to provide much direct guidance.

In computational studies, such as the present one, finite computational resources restrict the Reynolds numbers that can be addressed. The implementation of turbulence models and large-eddy simulation calculations is a natural next step and is being carried out.[8] Besides computations, experiments are appealing for many applications because they can provide rapid answers at realistic flow

conditions. Such a study has been initiated by the authors inspired by the present results.

The future role of computations in such optimizations is to address issues where experiments are limited. For example, consider the optimization of the physical shape of realistic actuators. It would be difficult to design hardware with the flexibility to provide a general shape for the actuation. However, in a simulation, it is straightforward to implement actuators of nearly any shape, and they may be constrained so that determined optimal geometry is realizable in hardware. This way the final configuration can be built and applied.

References

[1]Rechenberg, I., *Evolutionsstrategie: Optimierung Technischer System nach Prinzipien der biologischen Evolution*, Fromman–Holzboog, Stuttgart, Germany, 1973, pp. 1–170.

[2]Michalewicz, Z., *Genetic Algorithms + Data Structures + Evolution Programs*, Springer-Verlag, Berlin, 1996, pp. 1–387.

[3]Schwefel, H.-P., *Evolution and Optimum Seeking*, Wiley, New York, 1995, pp. 105–118.

[4]Freund, J. B., and Moin, P., "Jet Mixing Enhancement by High-Amplitude Fluidic Actuation," *AIAA Journal*, Vol. 38, No. 10, 2000, pp. 1863–1870.

[5]Parekh, D. E., Kibens, V., Glezer, A., Wiltse, J. M., and Smith, D. M., "Innovative Jet Flow Control: Mixing Enhancement Experiments," AIAA Paper 96-0308, 1996.

[6]Lee, M., and Reynolds, W. C., "Bifurcating and Blooming Jets," Dept. of Mechanical Engineering, Rept. TF-22, Stanford Univ., Stanford, CA, Aug. 1995.

[7]Parekh, D., Leonard, A., and Reynolds, W. C., "Bifurcating Jets at High Reynolds Numbers," Dept. of Mechanical Engineering, Rept. TF-35, Stanford Univ., Stanford, CA, Dec. 1988.

[8]Hilgers, A., "Parameter Optimization in Jet Flow Control," Center for Turbulence Research Annual Research Brief, Center for Turbulence Research, Stanford Univ., Stanford, CA, 1999, pp. 179–194.

J. P. Gore
Associate Editor

General Attenuation Laws for Spherical Shock Waves in Pure and Dusty Gases

F. Aizik,* G. Ben-Dor,† T. Elperin,† and O. Igra†
Ben-Gurion University of the Negev, 84105 Beer Sheva, Israel

Introduction

THE most common shock wave in nature is a spherical one. This is the reason for the importance of knowing the flowfield that is developed behind a spherical shock wave. The full governing equations that describe the flowfield consist of nonlinear partial differential equations. Because of their complexity and unless simplifying assumptions are applied, they can be solved only numerically. The numerical solution requires significant resources (time, computers, etc.). The complexity of solving these equations on one hand, and the importance, in many applications, of knowing the flowfield properties in real time, on the other hand, was our motivation to develop an alternative way of obtaining the flowfield properties immediately behind the shock wave front.

Olim et al.,[1] in their study of the flowfield that is developed behind attenuating planar shock waves propagating in a dusty air, showed that the numerical simulation could be replaced by a semi-empirical relation describing the instantaneous shock wave Mach number, that is, the shock wave velocity divided by the speed of sound of the gaseous phase ahead of it.

The correlation proposed by Ref. 1 implied that the shock wave degenerated to a sound wave, that is, $M_s \to 1$, when $x \to \infty$ as, indeed, should the case be if the wave is unsupported. However, Sommerfeld[2] found in the course of his experimental investigation, which was conducted in a shock tube in a finite length domain, that if the initial shock wave was strong and the dust-loading ratio was low to moderate, the shock wave did not attenuate to a sound wave but to a finite strength shock wave whose Mach number was larger than unity.

Because of this observation, Aizik et al.[3] modified the attenuation law suggested in Ref. 1. Kurian and Das[4] recently reported good agreement when they compared predictions based on the modified attenuation law of Ref. 3 with their experimental results.

The purpose of the present study was to extend the studies just mentioned and develop two general attenuation laws for spherical shock waves propagating 1) in pure gases and 2) in particle-laden gases.

Present Study

Rupturing a spherical diaphragm inside which the pressure p_4 was higher than the ambient pressure p_1 and the temperature T_4 was higher or equal to the ambient temperature T_1 generated the spherical shock wave. The particles, in the gas–particle suspension case, were uniformly distributed outside the spherical diaphragm.

The governing equations describing the propagation of a spherical shock wave through both pure and particle-laden gases were formulated and solved numerically using the random choice method (RCM) with operator splitting technique.

The computer code was validated by comparing its predictions to all of the experimental results of Boyer.[5,6] Very good agreement was evident. Full details of the comparison can be found in Ref. 7, where a detailed derivation of the governing equations and their final form are also given. The assumptions on which the governing equations were based were as follows: 1) The flowfield is one-dimensional (radial) and unsteady. 2) The gaseous phase behaves as a perfect gas. 3) The solid particles, which are identical in all their physical properties, are rigid spherical and inert. They are uniformly distributed in the gaseous phase. 4) The number density of the solid particles is sufficiently high for considering the solid phase as a continuous medium. 5) The solid particles do not interact with each other. As a result, their partial pressure in the suspension is negligibly small. 6) The volume occupied by be solid particles is negligibly small. 7) The heat capacity of the solid particles is constant. 8) The dynamic viscosity, the thermal conductivity, and the specific heat capacity at constant pressure of the gaseous phase depend solely on its temperature. 9) Other than the momentum and energy exchanges between the solid and the gaseous phases, the gaseous phase is assumed to be an ideal fluid, that is, inviscid and thermally nonconductive. 10) The weight of the solid particles and the buoyancy force are negligibly small compared to the drag force acting on them. 11) The solid particles are too large to experience a Brownian motion. 12) The temperature within the solid particles is uniform.

General Attenuation Law of Spherical Shock Waves Propagating in Pure Gases

The governing equations were solved numerically for a variety of initial conditions, to identify the parameters affecting the spherical shock wave attenuation. As expected, in the case of a pure gas, the most dominant parameter was its initial strength, that is, the initial Mach number, which can be derived from the pressure and the temperature ratios ($P_{41} = p_4/p_1$ and $T_{41} = T_4/T_1$, respectively) across the spherical diaphragm (e.g., see Ref. 8).

The numerical results indicated that an exponential curve could well fit the primary spherical shock wave attenuation. In addition, it is well known that spherical shock waves degenerate to sound waves far away from their origin. Under this constraint the spherical shock wave attenuation was described by

$$M_s = (M_{s,0} - 1)\exp[-(r - r_0)/\Re] + 1 \qquad (1)$$

Received 26 October 1999; revision received 20 October 2000; accepted for publication 20 December 2000.

*Graduate Student, Department of Mechanical Engineering.

†Professor, Pearlstone Center for Aeronautical Engineering Studies, Department of Mechanical Engineering.